Macromolecules
ARTICLE

Macromolecules **2010**, *43*, 1515–1523 **1515**
DOI: 10.1021/ma902343m

Dynamic Signatures of Microphase Separation in a Block Copolymer Melt Determined by X-ray Photon Correlation Spectroscopy and Rheology

Amish J. Patel,[†] Simon Mochrie,[‡] Suresh Narayanan,[§] Alec Sandy,[§] Hiroshi Watanabe,*[,∥] and Nitash P. Balsara*[,†,⊥]

[†]*Department of Chemical Engineering, University of California, Berkeley, California 94720,* [‡]*Department of Physics, Yale University, New Haven, Connecticut 06520,* [§]*Argonne National Laboratory, Argonne, Illinois 60439,* [∥]*Institute for Chemical Research, Kyoto University, Uji, Kyoto 611-0011, Japan, and* [⊥]*Materials Sciences Division and Environmental Energy Technologies Division, Lawrence Berkeley National Laboratory, University of California, Berkeley, California 94720*

Received October 21, 2009; Revised Manuscript Received December 8, 2009

ABSTRACT: The relationship between structure and dynamics in a polystyrene-polyisoprene block copolymer melt in the vicinity of the order−disorder transition was studied by small-angle X-ray scattering (SAXS), X-ray photon correlation spectroscopy (XPCS), and rheology. Rheological measurements on the disordered state indicate the presence of a fast process arising from the relaxation of polyisoprene chains and a slow process resulting predominantly from the relaxation of concentration fluctuations. In contrast, XPCS measurements of the disordered phase are dominated by diffusion of micelles. Time-resolved SAXS, XPCS, and rheology experiments on samples quenched from disorder-to-order reveal the existence of two regimes. While the microscopic relaxation time, measured by XPCS, increases after all of the quenches, SAXS and rheological signatures of ordering are only seen when the quench depth exceeds a critical value of 10 °C. For quenches 5 °C below the order-to-disorder transition temperature, no changes in the SAXS profiles and rheological properties are observed on experimental time scales. It is evident that nucleation barriers preclude the formation of the ordered phase during shallow quenches. The time-resolved rheology measurements enable estimation of the nucleation barriers that are responsible for the observations in the shallow quench regime.

Introduction

Much of our understanding of block copolymers is based on static data obtained by techniques such as diffraction, birefringence, and electron microscopy.[1−7] While techniques such as rheology[8] and dielectric spectroscopy[9] have been used to characterize the dynamics of block copolymers, insight into molecular scale dynamic processes that occur in these systems is limited. This is because these techniques measure the overall response of all of the molecules in the system to applied external fields (stress, strain, or electric fields). Because of aggregation of the molecules into structures such as micelles, hexagonally packed cylinders, and alternating lamellae, the collection of inter- and intramolecular relaxation processes that are available to the system is very large. It has proven difficult to isolate the contributions of the individual processes to the overall response. It is known, for example, that temperature-dependent rheological data from disordered block copolymers do not obey time−temperature superposition, and while this behavior is partly attributed to a difference in the activation energies of the component dynamics,[10−13] a quantitative understanding of the reason for this departure has not been identified in most cases.

Techniques such as neutron spin echo (NSE), light photon correlation spectroscopy (LPCS), and X-ray photon correlation spectroscopy (XPCS) enable direct measurement of the dynamical structure factor. These techniques are instrumental in identifying individual relaxation processes[14−18] because they enable the quantification of relaxation times as a function of the magnitude of the scattering vector, q. NSE measurements in block copolymer melts have enabled the determination of fast relaxation processes (∼10 ns) arising from the collective relaxation behavior as well as from single chain relaxation.[18] LPCS studies on both disordered and ordered block copolymer solutions have led to an understanding of relaxation processes on length scales comparable to the wavelength of light.[19−30] In typical block copolymers, this length scale ($2\pi/q$) is significantly larger than molecular length scales, and LPCS therefore enables the study of diffusive processes and collective motions on these length scales. In an important study, Anastasiadis et al. studied the LPCS signal from a solution of a block copolymer with molecular weight of about 1000 kg/mol. In this case they were able to access dynamics on molecular length scales. They showed that the time scale of relaxation, τ, as a function of scattering vector, q, was peaked at the same location as the peak of the static structure factor.[31−33] This is qualitatively different from typical diffusive processes where τ is a monotonic function of q ($\tau \sim q^{-2}$). While this effect was predicted theoretically,[12,34] experimental demonstration of the fact that τ could in fact decrease as the characteristic length scale increases was a remarkable achievement.

The purpose of the present work is to determine $\tau(q)$ in a block copolymer system. There are four main differences when one compares the present study with the $\tau(q)$ determination in refs 31 and 33: (1) We use X-ray photon correlation spectroscopy (XPCS) which enables access to length scales of 20 nm compared to 500 nm accessed by LPCS. (2) We have studied the dynamics in a block copolymer melt while the systems studied in refs 31 and 33 are relatively dilute solutions of block copolymers (2.4−7.5 wt %). (3) We focus on an asymmetric copolymer that forms transient

*To whom correspondence should be addressed.

Published on Web 01/07/2010

micelles in the disordered state while the systems studied in refs 31 and 33 were symmetric block copolymers in a common solvent where micelles are absent in the disordered phase. (4) References 31 and 33 report on the dynamics above the order-to-disorder transition temperature (T_{ODT}), whereas we have conducted dynamic studies both above and below T_{ODT}.

In a previous study,[35] we used XPCS to probe the dynamics of a polystyrene-*block*-polyisoprene copolymer. In ref 35, we focused on data obtained in the disordered state where we were able to show that τ at the peak of the static structure factor was related to the diffusion of micelles that form and disappear spontaneously in the disordered state. We also demonstrated that the value of τ was orders of magnitude larger than the longest relaxation time measured by rheology. The main purpose of this paper is to report on measurements of τ in the ordered state. Not surprisingly, we find that τ is time-dependent as the copolymer melt transforms from disorder to order. Analysis of this data enables tracking the evolution of the relaxation processes in the block copolymer melt as it transforms from disorder to order. It is worth noting that virtually all of our knowledge of the disorder-to-order transformation is based on quasi-static structural probes such as time-resolved scattering, microscopy, and birefringence.[2−6,36] While rheology is often used to track this transformation, the rheological changes are usually recast in terms of qualitative predictions of the static structure.[8,36−40]

Experimental Section

We have studied a polystyrene-*block*-polyisoprene copolymer, SI(7−27), which was synthesized by anionic polymerization under high vacuum. The weight-averaged molecular weights of the polystyrene and polyisoprene blocks were determined to be 6.7 and 26.5 kg/mol, respectively. The volume fraction of the polystyrene block is 0.179. Our synthesis and characterization procedures are given in ref 41. Both SAXS and XPCS data from SI(7−27) melts were obtained at the 8-ID-I beamline at the Advanced Photon Source (APS) at Argonne National Laboratory. The block copolymer was placed in a 1 mm diameter hole in a 3 mm thick aluminum plate. The polymer did not flow out of the hole in spite of the absence of windows and repeated cycling through the order−disorder transition temperature. The plate was housed in a cell capable of controlling the temperature (T) within ±0.1 °C in the $30 < T < 200$ °C range. The cross section of the X-ray beam was 20 μm × 40 μm, and the thickness of the sample was ca. 3 mm. Several "spots" on each sample were examined during the course of an experiment. The sample thickness at each spot was determined up to a constant by applying Beer's law to the measured local transmission coefficient. The scattering intensity, I, is reported in arbitrary units (a.u.) after accounting for differences in sample thickness. Rheological measurements on SI(7−27) were conducted using an ARES Rheometer (Rheometrics Inc.). The sample was held between 8 mm diameter parallel plates that were heated to the set temperature. In addition, the sample chamber had a steady flow of nitrogen gas in order to maintain an inert atmosphere around the sample. Because of the relatively large thermal mass of the polymer sample, the conduction of heat out of the sample chamber due to intimate contact with large rheological fixtures, and the presence of convection inside the sample chamber, temperature gradients across the sample are expected to be much larger in the rheological experiments than in the X-ray experiments. In order to get an accurate estimate of the sample temperature for both rheology and XPCS experiments, we performed a calibration procedure where we inserted a thermocouple inside the polymer sample. We were thus able to obtain a correspondence between the set temperature and the sample temperature measured by the thermocouple.

The structure and thermodynamic properties of SI(7−27) melts were determined using a combination of SAXS, birefringence, and rheology.[42] The system undergoes an ODT at a temperature, $T_{ODT} = 70 \pm 2$ °C. Below T_{ODT}, the system exists as a hexagonally packed cylinder phase at equilibrium and above T_{ODT}, it is disordered and contains disordered micelles. The volume fraction of these micelles was estimated to be less than 7% near and above the ODT, and it decreases as the temperature is increased. We see no signature of the presence of micelles at temperatures above 100 °C.[35,42]

The main purpose of this paper is to report on the dynamical properties of SI(7−27) measured by XPCS. We present time-dependent XPCS data obtained after the sample was thermally quenched from the disordered to the ordered state. We report the results from two types of quench experiments: single-step and two-step quenches. In the single-step experiments, we quench the sample directly from the disordered to the ordered state. In the two-step quench experiments, we quench the disordered sample to a certain quench depth in the ordered state, wait for a certain amount of time, and then reduce the quench depth by increasing sample temperature. All our XPCS experiments were started by annealing the sample at a temperature of 120 °C or higher for 60 min. The rheology experiments were started by annealing the sample at 100 °C or higher for 60 min. This is above the temperature where the sample is completely disordered and does not exhibit any detectable signatures of disordered micelles. The quenches from 120 °C (for XPCS) and 100 °C (for rheology) to various temperatures in the ordered regime were executed in less than 10 min. Quench time, t, is defined as the time spent by the sample in the ordered state, and $t = 0$ is defined as the time at which the sample temperature reaches within 0.1 °C of the target quench temperature. Quench depth, ΔT, is defined as the difference between T_{ODT} and the sample temperature, T. The annealing protocol for the XPCS measurements is a little more conservative than that used in the rheological experiments. We found that the initial annealing temperature had no effect on rheology and thus used 100 °C as the annealing temperature. As we learned about the system by XPCS, we increased the annealing temperature to 120 °C, to ensure a micelle-free initial starting point.

Data Analysis

XPCS was used to measure the dynamic structure factor, $S(q,t_d)$, in the vicinity of q^*, the peak of the static structure factor, where t_d is the delay time which should not be confused with quench time t. If a single process dominates the relaxation of concentration fluctuations, i.e., $S(q,t_d) \sim \exp(-t_d/\tau_{fluc})$, the SAXS intensity time correlation function, $g_2(q,t_d)$, is given by

$$g_2(q,t_d) \equiv \frac{\langle I(q,0)I(q,t_d)\rangle}{\langle I(q,0)\rangle^2} = 1 + k\exp\left(-\frac{2t_d}{\tau_{fluc}(q)}\right) \qquad (1)$$

where $\tau_{fluc}(q)$ is the characteristic time for the relaxation of concentration fluctuations over a length scale $2\pi/q$ and k is an instrument constant. In all cases, the measured $S(q,t_d)$ exhibited single-exponential behavior, consistent with eq 1, and qualitatively similar to the data presented in ref 35. In this paper, we only report $\tau_{fluc}(q=q^*)$, which we shall refer to as τ_{fluc} from now on.

In ref 35 we reported on the XPCS signal from SI(7−27) in the disordered state (70−90 °C). In principle, the decay of concentration fluctuations in the disordered state could occur due to a variety of processes such as decorrelation of the unstable concentration fluctuations of the disordered state, dissolution and reappearance of micelles (finiteness of micelle lifetime), or diffusion of intact micelles. In this regime, we found that τ_{fluc} was independent of time. We demonstrated that it reflected the characteristic time for diffusion of intact micelles. The time scale τ_{SE} for the diffusion of an intact micelle over a distance equal to its radius R_H ($\approx 2\pi/q^*$) can be approximated using the

Stokes−Einstein relationship

$$\tau_{SE} = \frac{\pi R_H{}^3 \eta_{eff}(T)}{k_B T} \quad (2)$$

where η_{eff} is the effective viscosity of the medium, k_B is the Boltzmann constant, and T is the temperature.[43] In general, η_{eff} differs from the rheologically measured zero-shear viscosity, η_0, because the presence of micelles affects η_0. If, for example, the micelles can be approximated as hard spheres, then $\eta_0 = \eta_{eff}[1 + 2.5\phi_m + O(\phi_m{}^2)]$ with ϕ_m being the micelle volume fraction.[44] However, since we estimate the micelle volume fraction to be small[35] ($\phi_m < 0.07$) for $T > T_{ODT}$, we assume that $\eta_{eff} \approx \eta_0$ for evaluating τ_{SE} using eq 2. Since $\eta_{eff} < \eta_0$, the value of τ_{SE} estimated using eq 2 with $\eta_{eff} = \eta_0$ represents an upper bound on the actual value of τ_{SE}. This approach for estimating τ_{SE} is inapplicable in the $T < T_{ODT}$ regime because under most circumstances, the terminal regime cannot be accessed in rheological experiments, and the volume fraction of the transient micelles is expected to become large as the system transforms from disorder to order.[45,46] Lacking a better approximation, we obtain an upper bound for τ_{SE} by extrapolating the η_0 data in the $T > T_{ODT}$ region to $T < T_{ODT}$ and utilizing the extrapolated η_0 in eq 2. We make use of time−temperature superposition (TTS)[47] in order to obtain extrapolated values for η_0. A reference temperature (T_r) is chosen and G' and G'' data are shifted down vertically by an intensity correction factor, $b_T = T/T_r$, and horizontally to the right by a shift factor, a_T, chosen such that the shifted G' and G'' data overlap with data at the reference temperature, T_r.

Structurally complex systems such as block copolymers having distinct relaxation mechanisms with different temperature dependencies do not exhibit TTS in the entire frequency range.[8] However, if the characteristic time scale of the distinct processes are widely separated, then it may be possible to perform limited TTS analyses in limited frequency windows.[48] The temperature dependence of a_T is usually given by either the Arrhenius equation

$$a_T = \exp\left[\frac{\Delta E_a}{R}\left(\frac{1}{T} - \frac{1}{T_r}\right)\right] \quad (3)$$

where ΔE_a and R are the activation energy and the universal gas constant, respectively, or the Williams−Landel−Ferry (WLF) equation[47]

$$a_T = \exp\left[-2.303\frac{C_1(T - T_r)}{C_2 + T - T_r}\right] \quad (4)$$

where C_1 and C_2 are empirical constants.

G' and G'' are time-dependent as the samples transform from disorder to order. Immediately after quenching the sample, the system shows terminal behavior, and the time dependence of the storage modulus at the lowest measured angular frequency (ω = 0.01 rad/s) is sigmoidal as reported in the literature;[49] i.e., it remains constant initially (induction time), rises sharply, and finally reaches a plateau at long times. To obtain a crude estimate of the nucleation time, τ_n, for the formation of the ordered phase, we fit the early time data (times when the G' vs t slope increases with time) to the following functional form

$$G'_{fit}(t) = c + k\left\{\exp\left(\frac{t}{\tau_n}\right) - \frac{t}{\tau_n}\right\} \quad (5)$$

where c, k, and τ_n are fitting parameters, and the linear term in the curly brackets has been subtracted to ensure that the functional form captures the experimental observation that $G'(t)$ has zero slope at $t = 0$.

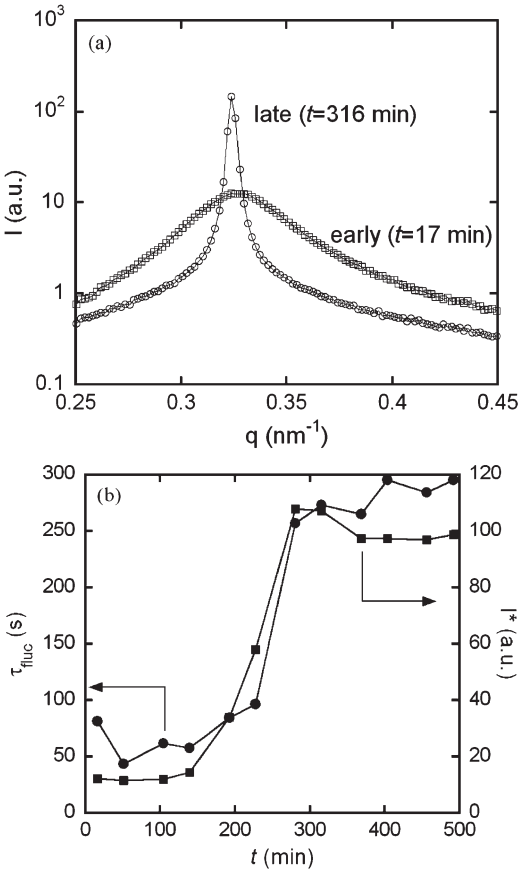

Figure 1. (a) Static SAXS intensity, I, vs magnitude of the scattering vector, q, at early, t = 17 min (squares), and late, t = 326 min (circles), times after a deep quench to 60 °C. (b) τ_{fluc} (left ordinate, circles)[50] and I^* (right ordinate, squares) as a function of quench time, t, for the deep quench. The sharp increase in both the curves between a quench time of ~120 and ~280 min is a result of the microphase separation transition.

Results and Discussion

SAXS and XPCS. We performed time-resolved SAXS and XPCS experiments on the SI(7−27) melt after quenching the sample from the disordered state to several temperatures below the order−disorder transition temperature (T_{ODT}). In Figure 1, we show the results from time-resolved SAXS for a quench to 60 °C. We call this the *deep quench*, since results obtained from all other quenches to lower temperatures (down to 50 °C) showed qualitatively similar results. Figure 1a contrasts the static scattering profile, $I(q)$, at quench times soon after the quench was completed (t = 17 min) with that obtained at t = 316 min. The t = 17 min $I(q)$ profile shows a broad peak with a small value of I at the peak, I^*, in the vicinity of 10 a.u. At t = 316 min, we see a SAXS profile with a sharp peak and I^* is about 100 a.u. This is typical of a block copolymer melt that has undergone an ODT. In Figure 1b, we plot I^* (squares) as a function of quench time t. This figure clearly indicates that microphase separation starts at t = 120 min and is completed at t = 280 min. Also shown in Figure 1b is the time dependence of τ_{fluc}, measured by XPCS (circles). There is a remarkable similarity in the time dependencies of τ_{fluc} and I^*. τ_{fluc} increases rapidly from its disordered value of 50 s at t = 120 min and reaches a plateau at $t \approx 280$ min. There is little doubt that the time dependence of τ_{fluc} is due to the

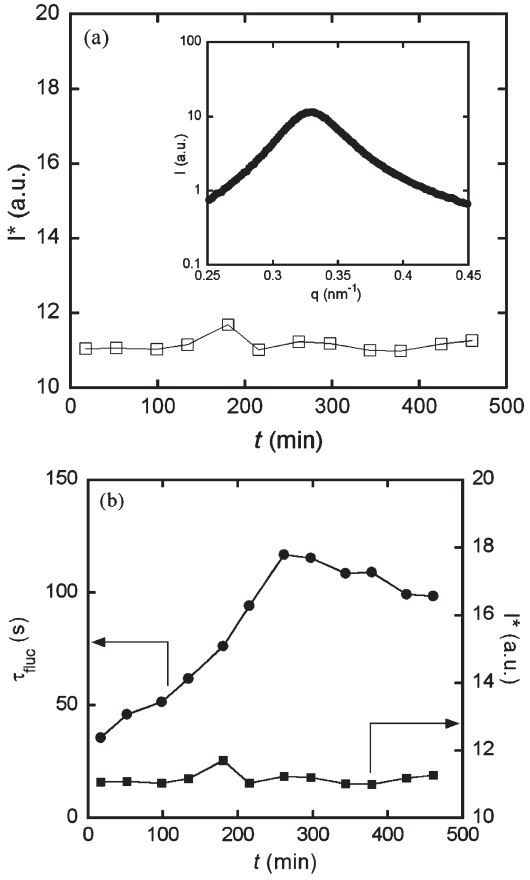

Figure 2. (a) Peak SAXS intensity, I^*, vs quench time, t, after a shallow quench to 65 °C. I^* does not change for up to $t = 480$ min. The inset shows the static SAXS intensity, I, vs magnitude of the scattering vector, q, at $t = 18$ and 420 min. The broad peak and the complete overlap of the different data sets indicate that the system remains disordered throughout this time. (b) τ_{fluc} (left ordinate, circles)[50] and I^* (right ordinate, squares) as a function of quench time, t, for the shallow quench. While I^* does not change with quench time, τ_{fluc} increases gradually until $t = 250$ min.

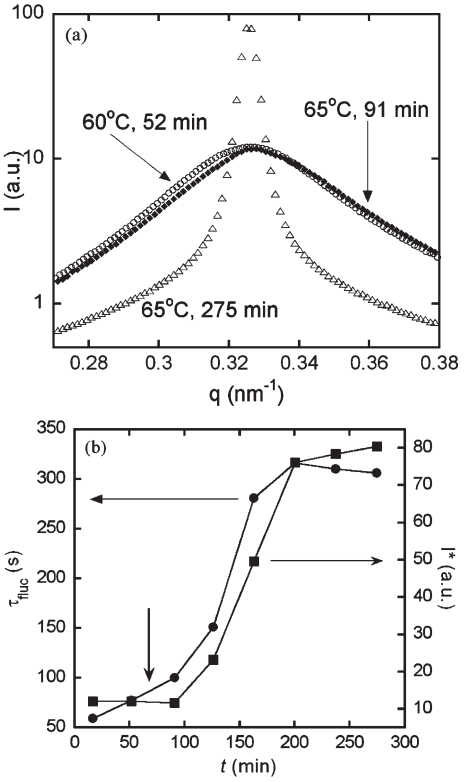

Figure 3. (a) Static SAXS intensity, I, vs magnitude of the scattering vector, q, at various times during the two-step quench: after the first quench to 60 °C at $t = 52$ min (open circles), early after the second quench to 65 °C at $t = 91$ min (filled diamonds), and at late times after the second quench at $t = 275$ min (open triangles). The first quench to 60 °C results in the formation of nuclei, which are able to grow after the quench temperature was changed to 65 °C. (b) τ_{fluc} (left ordinate, circles)[50] and I^* (right ordinate, squares) as a function of quench time for the double quench. The vertical arrow indicates the time at which the quench temperature was changed from 60 to 65 °C.

disorder-to-order transition. Similar agreement between the time dependencies of τ_{fluc} and I^* was obtained at 55 and 50 °C. This may be considered as another manifestation of the result in ref 31 wherein structure and dynamics at q^* are strongly coupled. For both 50 and 55 °C quenches, the final value of $\tau_{fluc} \sim 300$ s. Different runs of quenches to the same temperature resulted in slightly different time dependencies of I^* and τ_{fluc}. For example, for quenches to 60 °C, the time required to reach the midpoint between the values of τ_{fluc} characteristic of the disordered and ordered states ranged from 200 to 400 min. We attribute this to our inability to exert exact control over the thermal history of the sample due to variability of sample thickness, proximity to the container wall, etc. In spite of this, the strong coupling between I^* and τ_{fluc} was observed in all cases.

In Figure 2, we show results obtained from a quench to 65 °C, which we call the *shallow* quench. The inset of Figure 2a shows a scattering profile with a broad peak and a small value of I^* (~10 a.u.), indicative of a disordered state. There is no detectable change in this SAXS profile for t values ranging from 0 to 480 min. Given the fact that we have used an instrument with excellent resolution, we conclude that the shallow quench was unsuccessful in forming an ordered phase on experimental time scales. This is undoubtedly due to the fact that nucleation barriers are large when the quench depth is 5 °C. Figure 2b compares the time dependencies of I^* and τ_{fluc} at the same shallow quench to 65 °C. In contrast to I^*, τ_{fluc} exhibits a substantial increase from 35 to 100 s during the first 250 min. The time dependence of τ_{fluc} and I^* are remarkably uncorrelated under shallow quench conditions. Since I^* and τ_{fluc} are extracted from the same set of 2-D scattering data, this lack of correlation cannot be attributed to an experimental artifact. The result seen in Figure 2b cannot be anticipated from any previous studies on ordering kinetics in block copolymers.[51−60] We repeated the 65 °C quench numerous times and always got the same result.

To confirm that nucleation barriers at low quench depths preclude completion of the disorder-to-order transition at 65 °C on experimental time scales, we performed a two-step quench experiment.[61] We initially quenched the system to 60 °C and kept the system at 60 °C for 60 min, before heating the sample to 65 °C. The parameters for the first step were chosen due to the fact that no signatures of order formation are seen at 60 °C when $t < 60$ min (Figure 1b). The SAXS data obtained near the end of the first quench ($t = 52$ min), shown in Figure 3a, are very similar to the disordered state data shown in Figures 1a (early) and 2a. The data obtained just after the sample temperature was increased to 65 °C at $t = 91$ min are also shown in Figure 3a. There no qualitative difference between the data obtained before and just after the second quench. However, over time, we find a dramatic increase in I^* and a sharp primary peak characteristic of the ordered phase is seen at $t = 275$ min. In Figure 3b we show the time dependence of τ_{fluc} and I^* after the two-step quench to 65 °C. There is excellent correlation between

τ_{fluc} and I^*, after the two-step quench to 65 °C, as was the case after a one step quench to 60 °C. It is clear that the first quench to 60 °C causes the creation of nuclei that grow readily at 65 °C. Note that the values of τ_{fluc} obtained after the two-step quench to 65 °C are around 300 s, which is similar to those obtained after a one-step quench to 60 °C.

Rheology. The equilibrium G' and G'' at $T > T_{ODT}$ for SI(7−27) were shown in ref 35 to exhibit terminal behavior at low frequencies. We also reported that the data over the entire frequency range could not be collapsed into a single master curve using TTS. This finding is consistent with all previous rheological studies of disordered block copolymers.[8,10,39,47] It is apparent that there are at least two distinct relaxation processes in disordered SI(7−27): a fast process contributing primarily to the high-frequency modulii and a slow process contributing to the low-frequency modulii.

We performed time-resolved rheological experiments on the SI(7−27) melt after quenching the sample from the disordered state to several temperatures below T_{ODT}. We performed TTS for the fast relaxation process with the reference temperature (T_r) chosen to be 90 °C as in ref 35. The G' and G'' data were reduced by an intensity correction factor $b_T = T/T_r$ and shifted along the frequency-axis to achieve the best superposition of the G'' data at high frequency. The TTS results for G' and G'' are shown in parts a and b of Figure 4, respectively. Equilibrium data obtained from the disordered state at $T > T_{ODT}$ and the early time-metastable-disordered phase data obtained at $T < T_{ODT}$ are shown. The temperature dependence of the horizontal shift factor, $a_{T,fast}$, used in this superposition is shown in Figure 4c. Excellent superposition is achieved for the high-frequency part of the G'' data (Figure 4b). The superposition with the same $a_{T,fast}$ is not perfect for G' (Figure 4a) due to the limited frequency window of our experiments. The solid curves (without data symbols) in Figure 4 represent the G' and G'' data (divided by b_T) obtained from a monodisperse six-arm polyisoprene (sPI) star polymer with an arm molecular weight, M_a = 23.5 kg/mol, at a temperature of 82 °C taken from ref 62. The molecular weight of the polyisoprene in the SI(7−27) diblock, M_{bI} = 26.5 kg/mol, is close to M_a of the star polymer, and the effect of the slight difference between T_r = 90 and 82 °C is known to have a negligible effect on the rheology of rubbery polysioprene. G' and G'' from sPI match well with those from SI(7−27). The fast relaxation observed at high frequencies in SI(7−27) can thus be attributed to the relaxation of the individual polyisoprene blocks. This has also been reported to be the case for a random dispersion of spherical styrene−isoprene micelles having polyisoprene coronae.[48,63] The $a_{T,fast}$ data shown in Figure 4c describe the temperature dependence of the relaxation time for the polyisoprene blocks. The temperature dependence is well described by both the WLF equation (eq 4) and the Arrhenius equation (eq 3) as indicated by excellent agreement of the experimental data with the fits (shown by dashed curves) in the entire temperature range covered. Thus, the dynamical process underlying the fast relaxation is unaffected by the order−disorder transition. The contribution of this process to the zero-shear viscosity of the medium, η_I, is given by $\eta_I(T) = \eta_{0,star} a_{T,fast} b_T$, where $\eta_{0,star}$ = 140 Pa·s, is the zero-shear viscosity of sPI. The terminal behavior of SI(7−27) is dominated by the slow process, and hence it is necessary to use the terminal viscosity of sPI to evaluate the contribution of the fast process to the terminal viscosity.

Figure 5 shows TTS for the slow process (terminal relaxation). The low-frequency G' values shown in Figure 5a

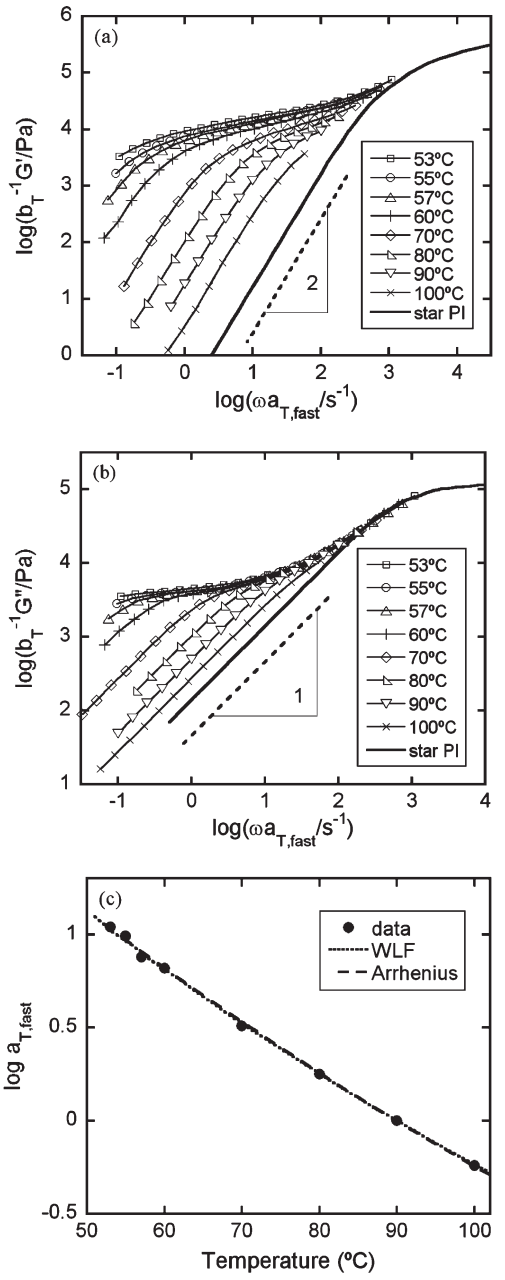

Figure 4. Time−temperature superposed (TTS) (a) G' and (b) G'' for the fast relaxation plotted as a function of reduced frequency $\omega a_{T,fast}$. The reference temperature for TTS is 90 °C. (c) $a_{T,fast}$ plotted as a function of temperature. The dashed lines are fits to the Arrhenius equation with ΔE_a = 63.1 kJ/mol and the WLF equation with C_1 = 7.2 K^{-1} and C_2 = 295 K.

exhibit excellent superposition, using shift factors $a_{T,slow}$. Applying the same shift factors to the G'' data results in unsatisfactory collapse as shown in Figure 5b. This is due to contamination from the fast relaxation tail, $G''_{fast} = \eta_I \omega$. Since the contribution to G' from the fast relaxation process, G'_{fast}, is proportional to ω^2, it is negligible at low frequencies. We thus define $\Delta G'' = G'' - G''_{fast}$, the contribution to G'' from the slow process, free of contamination from the fast process.[48] $\Delta G''$ shown in Figure 5c demonstrates excellent superposition using $a_{T,slow}$ shift factors. The temperature dependence of $a_{T,slow}$ common for both G' and $\Delta G''$ is shown in Figure 5d (left ordinate). The terminal relaxation time, τ_{tr}, is given by $\tau_{tr}(T) = \tau_{tr}(T_r) a_{T,slow}$, where $\tau_{tr}(T_r)$ = 0.049 s is the terminal relaxation time at the reference temperature (90 °C).

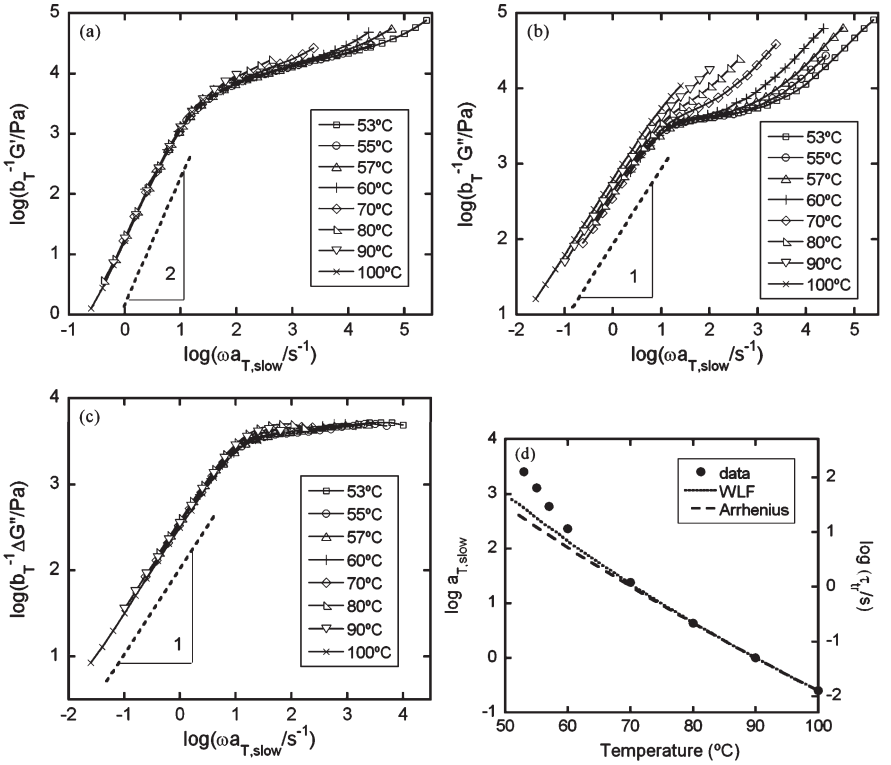

Figure 5. Time−temperature superposed (TTS) (a) G' (b) G'' and (c) $\Delta G''$ for the slow relaxation plotted as a function of reduced frequency $\omega a_{T,\mathrm{slow}}$. The reference temperature for TTS is 90 °C. The dashed lines with slopes 2 and 1 confirm that the system obeys terminal behavior at high temperatures. (d) $a_{T,\mathrm{slow}}$ (left ordinate) and terminal relaxation time, τ_{tr} (right ordinate), plotted as a function of temperature. The dashed lines are fits of the disordered state data to the Arrhenius equations with $\Delta E_a = 158$ kJ/mol and the WLF equation with $C_1 = 14\ \mathrm{K}^{-1}$ and $C_2 = 227$ K.

TTS thus enables estimation of τ_{tr} at the lower temperatures, where we do not observe terminal behavior in the experimentally available frequency window. τ_{tr} thus determined is shown in Figure 5d (right ordinate).

The temperature dependence of $a_{T,\mathrm{slow}}$ was fit to the WLF and Arrhenius equations. Neither form fits the data well over the entire temperature range. The WLF and Arrhenius fits shown in Figure 5d are thus only based on the $T > T_{\mathrm{ODT}}$ data. For $T > T_{\mathrm{ODT}}$, it was shown that the slow process (terminal relaxation) is due to the relaxation of concentration fluctuations of the disordered state.[35] The $a_{T,\mathrm{slow}}$ values are greater than those predicted by the empirical equations for $T < T_{\mathrm{ODT}}$, indicating a further slowing down on crossing the order−disorder transition. The volume fraction of the micelles in the metastable disordered fluid below T_{ODT} is expected to increase dramatically with decreasing temperature.[45,46] Since the WLF and Arrhenius equations do not account for this effect, we propose that the difference between the symbols ($a_{T,\mathrm{slow}}$) and the curves in Figure 5d reflects the growing concentration of disordered micelles.

In Figure 6a,b, we show the time dependence of $G'(\omega,t)$ and $G''(\omega,t)$ at $\omega = 0.01$ rad/s after quenches to temperatures between 50 and 70 °C. As is the case with previous studies of rheological properties of block copolymers across a disorder-to-order transition,[8,10] the signatures of order formation are more clearly seen in the G' data shown in Figure 6a. For the 57 °C quench, G' is independent of time at early times, begins to increase at $t \sim 600$ min, goes through an inflection ($t \sim 900$ min), and begins to level out at $t = 1320$ min, where the last measurement was made. This is the standard rheological signature of order formation.[49] As temperature is decreased, the same qualitative behavior is seen albeit with lower induction times and more rapid ordering kinetics. In spite of this, the early time $G'(t)$ plateau is clearly seen at both

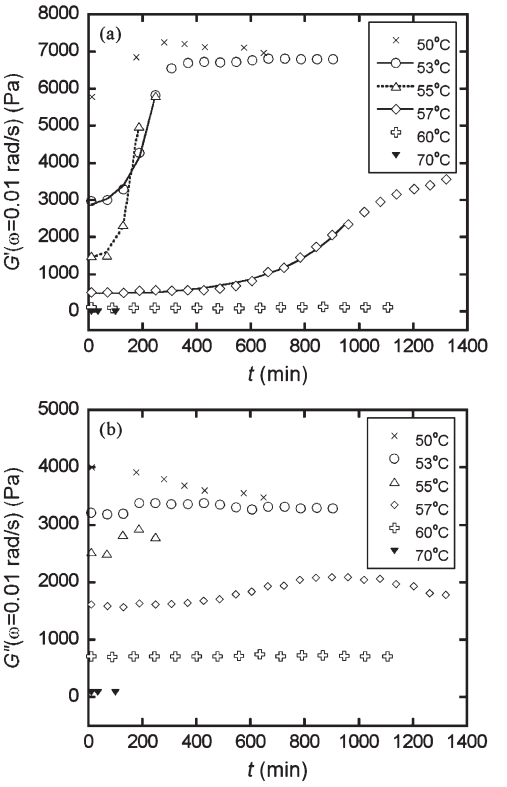

Figure 6. (a) G' and (b) G'' at $\omega = 0.01$ rad/s as a function of quench time, t, for quenches to temperatures between 50 and 70 °C. The curves in (a) are least-squares fits to the early time data using eq 5.

55 and 53 °C. At 50 °C, the early time $G'(t)$ plateau is outside the time resolution of our experiment, and only the last two

stages of order formation are discernible (Figure 6a). In contrast, both G' and G'' are independent of time during quenches to 60 and 70 °C, as shown in Figure 6.[64] As was the case with the SAXS and XPCS measurements, the rheological measurements also fall into two categories: data obtained from quenches to 57 °C and below where time-independent rheological data were obtained and quenches to 60 °C and above where time-dependent rheological data were obtained (Figure 6a). $T \leq 57$ °C is thus referred to as the deep quench regime while $T \geq 60$ °C is referred to as the shallow quench regime.

There is a slight discrepancy in the temperature at which the crossover from deep to shallow quench behavior is observed in the XPCS and rheology experiments. In XPCS the crossover is seen at 62.5 ± 2.5 °C while the rheological signatures of the crossover are seen at 58.5 ± 1.5 °C. We offer no substantive explanation for this discrepancy other than noting the fact that the sample environments in the two experiments are very different (see Experimental Section). This discrepancy may reflect uncontrolled differences in the two environments arising from differences in the temperature gradients or cooling rates. In spite of efforts to carefully calibrate the sample temperatures in both environments, as described in the Experimental Section, we were unable to obtain an exact correspondence between XPCS and rheology. Both XPCS and rheology experiments were repeated several times, and all of the measurements showed the same discrepancy noted above.

Analysis of Ordering Kinetics. The deep quench G' data in Figure 6a are used to estimate the time scales for nucleation, τ_n, using the method described in the Data Analysis section. The curves shown in Figure 6a are the least-squares fits of eq 5 to the early time data. Nucleation at $T = 50$ °C is too fast relative to the time it takes to quench our system, and at $T =$ 60 and 70 °C, it is too slow relative to experimental time scales. In Figure 7a, we plot τ_n as a function of quench depth, $\Delta T = T_{ODT} - T$, for $T =$ 53, 55, and 57 °C. At low quench depths, τ_n is expected to be large because the thermodynamic driving force for phase separation is small. At large quench depths, kinetic factors are expected to weigh in because molecular motion slows down as a result of the lower temperature. The nonmonotonic dependence of τ_n on ΔT seen in Figure 7a could be a consequence of this.

The time scale for order formation will depend on ΔW, the thermodynamic driving force for nucleation (in units of thermal energy) and the characteristic time for molecular motion. In the simplest case, we expect $\tau_n = C^{-1}\tau_{tr}\exp(\Delta W)$ with C being a constant. Since we have measured τ_n and τ_{tr} (Figures 7a and 5d), we can examine the dependence of ΔW on temperature. In Figure 7b, we show $\ln(\tau_n/\tau_{tr}) = \Delta W$ (ignoring the constant $-\ln C$) as a function of ΔT. ΔW is a decreasing function of ΔT. While the absolute magnitude of ΔW is unimportant due to the undetermined constant, C, the data in Figure 7b depict the dependence of the nucleation barrier on quench depth in the deep quench regime.

In the shallow quench regime, τ_{fluc} increases from 35 to 100 s over the first 250 min at 65 °C (Figure 2b). In contrast, the rheological time scale τ_{tr} (= 10 s, Figure 5d) does not change with quench time for at least 1100 min during the shallow quench (60 °C). We propose that this distinction arises from the fact that the XPCS signal is sensitive to the growing concentration of metastable micelles,[45] whereas the rheological signal is dominated by the disordered bulk, which does not change significantly with time at shallow quenches.

The results of our XPCS and rheology experiments obtained from both ordered and disordered systems are summarized in Figure 8. The circles in Figure 8a represent τ_{fluc} values measured at temperatures ≥70 °C where τ_{fluc} is independent of time. The triangles show values of τ_{fluc} obtained at $T < 70$ °C where τ_{fluc} depends on time. The dashed line in Figure 8a is a simple extrapolation of the disordered τ_{fluc} values to temperatures below T_{ODT}. One may view this extrapolation as the expected value of τ_{fluc} if a transition from disorder-to-order had not taken place. In ref 35 we showed that τ_{fluc} is dominated by the Stokes−Einstein diffusion of metastable micelles. At both 65 and 60 °C, the values of τ_{fluc} obtained at early times are smaller than that obtained from the extrapolation described above. This suggests that the diffusion of micelles in metastable disordered states is faster than that in stable disordered states due to differences in thermodynamic driving forces. With time, however, τ_{fluc} in the ordered state increases with time. The values of τ_{fluc} obtained at the end of the experiment, indicated by solid triangles in Figure 8a, are well above the extrapolations based on the disordered state. This is clearly consistent with the formation of an ordered state at 60 °C. We do not have a clear interpretation for the increasing τ_{fluc} at 65 °C because the SAXS data show no signs of order formation within this time window. It is conceivable that the dynamical signatures of order formation may precede static signatures in some systems. In a related study, Park et al.[65] found solidlike rheological properties in a cylinder-forming block copolymer solution when it was heated slightly above the ODT, even though all of the probes of static structure (SAXS and birefringence) indicated the lack of order. In their theoretical study of block copolymer melts, Wang et al.[66] have shown that asymmetric diblock copolymer melts quenched from the disordered to the ordered state can form a structural glass due to the existence of an exponentially large

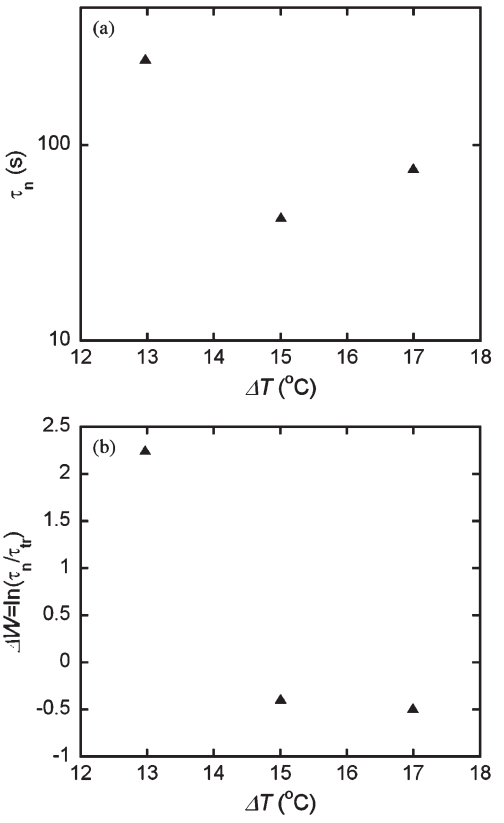

Figure 7. (a) Characteristic time for nucleation, τ_n, plotted as a function of quench depth, ΔT. (b) Thermodynamic driving force for nucleation, $\Delta W = \ln(\tau_n/\tau_{tr})$ (in units of thermal energy), as a function of quench depth, ΔT.

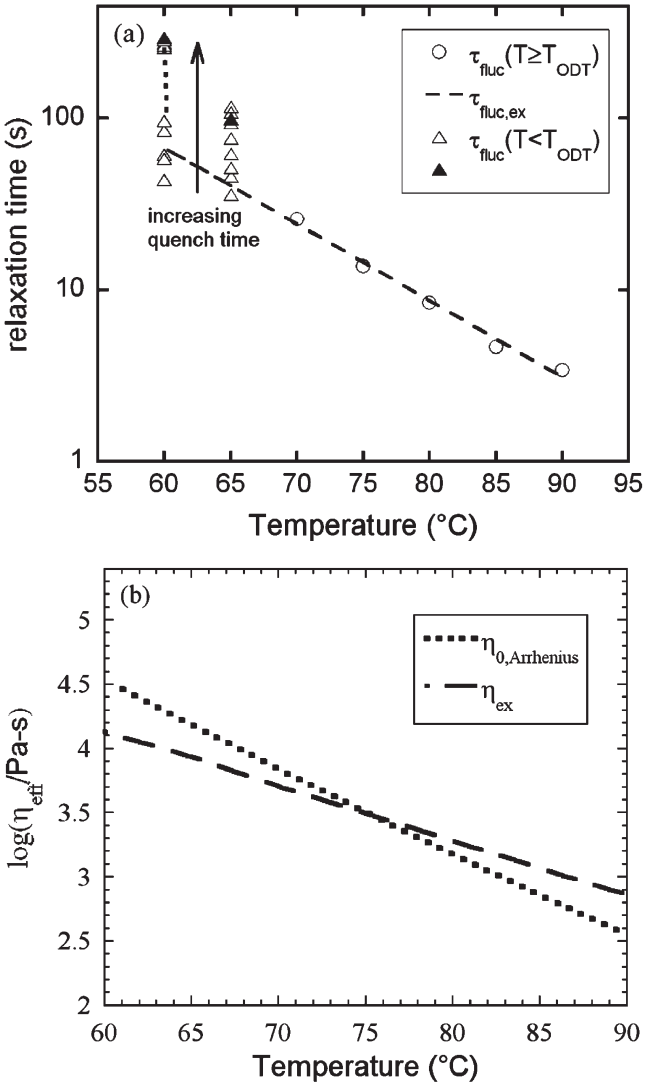

Figure 8. (a) Temperature dependence of the XPCS-measured relaxation time, τ_{fluc}, at $T < T_{ODT}$ (triangles) and $T \geq T_{ODT}$ (circles). τ_{fluc} at $T < T_{ODT}$ is time-dependent. The dashed line represents a simple extrapolation of the τ_{fluc} ($T \geq T_{ODT}$) data. (b) Approximations for the effective viscosity of the medium experienced by the micelles, plotted as a function of temperature.

number of metastable states consisting of random structures such as micelles. Perhaps the formation of such a structural glass, which cannot be detected by static structure measurements, is the reason for the lack of order formation at small quench depths (65 °C).

In Figure 8b, we compare measured viscosities of the disordered fluid using rheology and XPCS. The rheological viscosity is taken as $\eta_{0,Arrhenius}(T) = \eta(T_r)a_{T,slow,Arrhenius}b_T$, where $\eta(T_r) = 360$ Pa·s is the terminal viscosity of the sample at $T_r = 90$ °C. $a_{T,slow,Arrhenius}$ (Figure 5d) is obtained by fitting the disordered state $a_{T,slow}$ to eq 3 and represents our best approximation for the effective viscosity experienced by the micelles. The XPCS viscosity, η_{ex}, is obtained by using eq 2, the Stokes−Einstein relationship with $\tau_{SE} = \tau_{fluc,ex}$ (Figure 8a) and R_H determined from the peaks of the SAXS profiles.[35,45] The qualitative agreement between these two entirely independent viscosity measurements (Figure 8b) lends support to the proposed framework for describing fluctuation and stress relaxation in SI(7−27) melts. The quantitative disagreement seen in Figure 8b indicates that the framework is not perfect.

Conclusions

The relationship between structure and dynamics in a block copolymer melt in the vicinity of the order−disorder transition was studied by a combination of SAXS, XPCS, and rheology. The dynamical properties of the melt are affected by the presence of micelles that are stable at $T > T_{ODT}$ and metastable at $T < T_{ODT}$. A TTS-based methodology was applied separately to low- and high-frequency rheology data to estimate the viscosity of the melt surrounding the micelles. Our studies of ordering kinetics revealed the existence of two qualitatively different regimes, which we refer to as shallow and deep quench regimes. In the deep quench regime, the system undergoes conventional microphase separation as evidenced by the increase in I^*, the concomitant decrease in the SAXS peak width, and a sigmoidal increase in G'. Order formation is also accompanied by an increase in the microscopic relaxation time, τ_{fluc}, measured by XPCS. In the shallow quench regime, nucleation barriers preclude the formation of an ordered phase, and no changes in I^*, SAXS peak width, or G' are observed. However, τ_{fluc} increases with time and appears to level at long times. This lack of correlation between microscopic structure and dynamics was unexpected, and more work is needed to fully understand the underpinnings of this observation. By performing two-step quenches, a first short time quench into the deep quench regime followed by a second quench into the shallow quench regime, we demonstrated that the shallow quench behavior is due to the presence of nucleation barriers and not slow growth. In the deep quench regime, we obtained an estimate of the characteristic time for nucleation and identified the individual contributions from the kinetic factors and the activation barriers to nucleation.

Acknowledgment. Financial support was provided by the National Science Foundation (DMR 0453856). The APS is supported by the U.S. DOE under Contract W-31-109-Eng-38. A.J.P. gratefully acknowledges the graduate researcher fellowship from Tyco Electronics.

References and Notes

(1) Bates, F. S. *Macromolecules* **1985**, *18*, 525–528.
(2) Bates, F. S.; Fredrickson, G. H. *Annu. Rev. Phys. Chem.* **1990**, *41*, 525–557.
(3) Bates, F. S.; Fredrickson, G. H. *Phys. Today* **1999**, *52*, 32–38.
(4) Hamley, I. W. *The Physics of Block Copolymers*; Oxford University Press: Oxford, 1998.
(5) Balsara, N. P.; Perahia, D.; Safinya, C. R.; Tirrell, M.; Lodge, T. P. *Macromolecules* **1992**, *25*, 3896–3901.
(6) Balsara, N. P.; Garetz, B. A.; Dai, H. J. *Macromolecules* **1992**, *25*, 6072–6074.
(7) Hajduk, D. A.; Gruner, S. M.; Rangarajan, P.; Register, R. A.; Fetters, L. J.; Honeker, C.; Albalak, R. J.; Thomas, E. L. *Macromolecules* **1994**, *27*, 490–501.
(8) Bates, F. S.; Rosedale, J. H.; Fredrickson, G. H. *J. Chem. Phys.* **1990**, *92*, 6255–6270.
(9) Watanabe, H.; Urakawa, O.; Kotaka, T. *Macromolecules* **1993**, *26*, 5073–5083.
(10) Bates, F. S. *Macromolecules* **1984**, *17*, 2607–2613.
(11) Gouinlock, E. V.; Porter, R. S. *Polym. Eng. Sci.* **1977**, *17*, 535–543.
(12) Fredrickson, G. H.; Larson, R. G. *J. Chem. Phys.* **1987**, *86*, 1553–1560.
(13) Onuki, A. *Phys. Lett. A* **1977**, *64*, 115–116.
(14) Berne, B. J.; Pecora, R. *Dynamic Light Scattering*; Dover Publications: New York, 2000.
(15) Ngai, K. L.; Mashimo, S.; Fytas, G. *Macromolecules* **1988**, *21*, 3030–3038.
(16) Brown, W.; Stepanek, P. *Macromolecules* **1993**, *26*, 6884–6890.
(17) Stepanek, P.; Brown, W. *Macromolecules* **1998**, *31*, 1889–1897.
(18) Montes, H.; Monkenbusch, M.; Willner, L.; Rathgeber, S.; Fetters, L.; Richter, D. *J. Chem. Phys.* **1999**, *110*, 10188–10202.
(19) Fytas, G.; Anastasiadis, S. H.; Semenov, A. N. *Macromol. Symp.* **1994**, *79*, 117–124.

(20) Balsara, N. P.; Stepanek, P.; Lodge, T. P.; Tirrell, M. *Macromolecules* **1991**, *24*, 6227–6230.
(21) Kanetakis, J.; Fytas, G. *J. Non-Cryst. Solids* **1991**, *131*, 823–826.
(22) Anastasiadis, S. H.; Fytas, G.; Vogt, S.; Fischer, E. W. *Phys. Rev. Lett.* **1993**, *70*, 2415–2418.
(23) Vogt, S.; Jian, T.; Anastasiadis, S. H.; Fytas, G.; Fischer, E. W. *Macromolecules* **1993**, *26*, 3357–3362.
(24) Jian, T.; Anastasiadis, S. H.; Fytas, G.; Adachi, K.; Kotaka, T. *Macromolecules* **1993**, *26*, 4706–4711.
(25) Pan, C.; Maurer, W.; Liu, Z.; Lodge, T. P.; Stepanek, P.; Vonmeerwall, E. D.; Watanabe, H. *Macromolecules* **1995**, *28*, 1643–1653.
(26) Liu, Z.; Pan, C.; Lodge, T. P.; Stepanek, P. *Macromolecules* **1995**, *28*, 3221–3229.
(27) Stepanek, P.; Lodge, T. P. *Macromolecules* **1996**, *29*, 1244–1251.
(28) Hamersky, M. W.; Tirrell, M.; Lodge, T. P. *J. Polym. Sci., Part B: Polym. Phys.* **1996**, *34*, 2899–2909.
(29) Stepanek, P.; Almdal, K.; Lodge, T. P. *J. Polym. Sci., Part B: Polym. Phys.* **1997**, *35*, 1643–1648.
(30) Fleischer, G.; Rittig, F.; Stepanek, P.; Almdal, K.; Papadakis, C. M. *Macromolecules* **1999**, *32*, 1956–1961.
(31) Semenov, A. N.; Anastasiadis, S. H.; Boudenne, N.; Fytas, G.; Xenidou, M.; Hadjichristidis, N. *Macromolecules* **1997**, *30*, 6280–6294.
(32) Anastasiadis, S. H. *Curr. Opin. Colloid Interface Sci.* **2000**, *5*, 324–333.
(33) Chrissopoulou, K.; Pryamitsyn, V. A.; Anastasiadis, S. H.; Fytas, G.; Semenov, A. N.; Xenidou, M.; Hadjichristidis, N. *Macromolecules* **2001**, *34*, 2156–2171.
(34) Fredrickson, G. H. *J. Chem. Phys.* **1986**, *85*, 5306–5313.
(35) Patel, A. J.; Narayanan, S.; Sandy, A.; Mochrie, S. G. J.; Garetz, B. A.; Watanabe, H.; Balsara, N. P. *Phys. Rev. Lett.* **2006**, *96*, 258701.
(36) Hashimoto, T.; Ogawa, T.; Sakamoto, N.; Ichimiya, M.; Kim, J. K.; Han, C. D. *Polymer* **1998**, *39*, 1573–1581.
(37) Hahn, H.; Lee, J. H.; Balsara, N. P.; Garetz, B. A.; Watanabe, H. *Macromolecules* **2001**, *34*, 8701–8709.
(38) Hashimoto, T.; Shibayama, M.; Kawai, H.; Watanabe, H.; Kotaka, T. *Macromolecules* **1983**, *16*, 361–371.
(39) Watanabe, H.; Matsumiya, Y.; Kanaya, T.; Takahashi, Y. *Macromolecules* **2001**, *34*, 6742–6755.
(40) Adams, J. L.; Quiram, D. J.; Graessley, W. W.; Register, R. A.; Marchand, G. R. *Macromolecules* **1996**, *29*, 2929–2938.
(41) Lin, C. C.; Jonnalagadda, S. V.; Kesani, P. K.; Dai, H. J.; Balsara, N. P. *Macromolecules* **1994**, *27*, 7769–7780.
(42) Abuzaina, F. M.; Patel, A. J.; Mochrie, S.; Narayanan, S.; Sandy, A.; Garetz, B. A.; Balsara, N. P. *Macromolecules* **2005**, *38*, 7090–7097.
(43) Matsumiya, Y.; Watanabe, H. *Macromolecules* **2004**, *37*, 9861–9871.
(44) Einstein, A. *Ann. Phys.* **1906**, *19*, 289–306.
(45) Wang, J. F.; Wang, Z. G.; Yang, Y. L. *Macromolecules* **2005**, *38*, 1979–1988.
(46) Park, M. J.; Char, K.; Bang, J.; Lodge, T. P. *Macromolecules* **2005**, *38*, 2449–2459.
(47) Ferry, J. D. *Viscoelastic Properties of Polymers*; Wiley: New York, 1980.
(48) Watanabe, H. *Acta Polym.* **1997**, *48*, 215–233.
(49) Floudas, G.; Pakula, T.; Fischer, E. W.; Hadjichristidis, N.; Pispas, S. *Acta Polym.* **1994**, *45*, 176–181.
(50) The error bars for the relaxation times for a particular quench experiment are about 10%.
(51) Balsara, N. P.; Garetz, B. A.; Chang, M. Y.; Dal, H. J.; Newstein, M. C. *Macromolecules* **1998**, *31*, 5309–5315.
(52) Balsara, N. P. *Curr. Opin. Solid State Mater. Sci.* **1999**, *4*, 553–558.
(53) Chang, M. Y.; Abuzaina, F. M.; Kim, W. G.; Gupton, J. P.; Garetz, B. A.; Newstein, M. C.; Balsara, N. P.; Yang, L.; Gido, S. P.; Cohen, R. E.; Boontongkong, Y.; Bellare, A. *Macromolecules* **2002**, *35*, 4437–4447.
(54) Chastek, T. Q.; Lodge, T. P. *J. Polym. Sci., Part B: Polym. Phys.* **2006**, *44*, 481–491.
(55) Dai, H. J.; Balsara, N. P.; Garetz, B. A.; Newstein, M. C. *Phys. Rev. Lett.* **1996**, *77*, 3677–3680.
(56) Kim, W. G.; Garetz, B. A.; Newstein, M. C.; Balsara, N. P. *J. Polym. Sci., Part B: Polym. Phys.* **2001**, *39*, 2231–2242.
(57) Luo, K. F.; Yang, Y. L. *J. Chem. Phys.* **2001**, *115*, 2818–2826.
(58) Newstein, M. C.; Garetz, B. A.; Balsara, N. P.; Chang, M. Y.; Dai, H. J. *Macromolecules* **1998**, *31*, 64–76.
(59) Nie, H. F.; Bansil, R.; Ludwig, K.; Steinhart, M.; Konak, C.; Bang, J. *Macromolecules* **2003**, *36*, 8097–8106.
(60) Shannon, R. F.; Glavicic, M. G.; Singh, M. A. *J. Macromol. Sci., Phys.* **1994**, *B33*, 357–371.
(61) Patel, A. J.; Balsara, N. P. *Macromolecules* **2007**, *40*, 1675–1683.
(62) Qiao, X. Y.; Sawada, T.; Matsumiya, Y.; Watanabe, H. *Macromolecules* **2006**, *39*, 7333–7341.
(63) Watanabe, H.; Sato, T.; Osaki, K.; Hamersky, M. W.; Chapman, B. R.; Lodge, T. P. *Macromolecules* **1998**, *31*, 3740–3742.
(64) At 70 °C, the lowest frequency at which we were able to obtain G' and G'' is 0.1 rad/s. However, at this frequency, the system already displays terminal behavior. Hence, we can extrapolate the data obtained at $\omega = 0.1$ rad/s to obtain G' and G'' at $\omega = 0.01$ rad/s. The 70 °C data shown in Figure 3 have been obtained by such an extrapolation.
(65) Park, M. J.; Char, K.; Lodge, T. P.; Kim, J. K. *J. Phys. Chem. B* **2006**, *110*, 15295–15301.
(66) Zhang, C. Z.; Wang, Z. G. *Phys. Rev. E* **2006**, 73.